RF controls based on carrier suppression detection with attosecond resolution

F. Ludwig,* J. Branlard, M. Hoffmann, U. Mavrič, H. Pryschelski, L. Springer, and H. Schlarb

Deutsches Elektronen-Synchrotron DESY, Notkestraße 85, 22607 Hamburg, Germany

(Received 9 December 2024; accepted 16 July 2025; published 31 July 2025)

This paper presents a radio frequency (rf) control system with attosecond resolution based on a carrier suppression interferometer operating a superconducting cavity at the Cryo Module Test Bench (CMTB). This novel application of the carrier suppression detector extends conventional heterodyne methods and improves the residual jitter of the regulated rf field in the cavity by more than one order of magnitude. The cavity operated at 1.3 GHz with a gradient of 8 MV/m and a loaded quality factor of 10^7. The setup achieved out-of-loop phase noise detection values of $\mathcal{L} = -180$ dBc/Hz at 10 kHz and $\mathcal{L} = -165$ dBc/Hz at 100 Hz with a time resolution of 189 as within an offset frequency range from 10 Hz to 1 MHz. The phase noise budget of subcomponents such as in-loop and out-of-loop detectors, high-power drive, microphonics, and the reference source is reported. The facility rf reference phase noise in the offset frequency range from 1 to 100 kHz is identified as the key noise contributor. Furthermore, the narrow-band cavity reduces the phase jitter experienced by the beam to just 116 as. The presented research combining conventional receivers with carrier suppression detectors in continuous wave operation is a key milestone toward attosecond resolution, in particular relevant for pump-probe experiments in free-electron laser facilities.

DOI: 10.1103/jhc3-dtzw

I. INTRODUCTION

Pump-probe experiments at free-electron lasers (FEL) providing sub-10 fs resolution require ultrashort electron beams with excellent stability in terms of phase space and timing jitter. This requires short- and long-term stable rf fields in the accelerating cavities located in the bunch compressors and a precise rf or optical reference distribution system. In FELs, electron beams are longitudinally compressed by introducing an energy chirp to the beam using off-crest acceleration. The beam is then transported through a magnetic chicane, which introduces an energy-dependent path length, causing trailing electrons to catch up with electrons in the bunch head. A first-order approximation of the timing jitter after the bunch compression stage, assuming an ideal magnetic chicane, is given below [1]

$$\sigma_{t,\mathrm{out}}^2 \approx \left(\frac{R_{56}}{c_0}\frac{\sigma_A}{A}\right)^2 + \left(\frac{C-1}{C}\right)^2\left(\frac{\sigma_\varphi}{c_0 k_{\mathrm{rf}}}\right)^2 + \left(\frac{1}{C}\right)^2 \sigma_{t,\mathrm{in}}^2, \tag{1}$$

where $\sigma_{t,\mathrm{in}}$ and $\sigma_{t,\mathrm{out}}$ are the incoming and outgoing arrival time jitter, σ_A and σ_φ are the rf amplitude and phase stability of the rf accelerating field prior to the chicane, C is the beam compression factor, R_{56} is the chicane momentum compaction factor, k_{rf} is the rf field wave number, and c_0 is the speed of light in vacuum. The correlated beam jitter $\sigma_{t,\mathrm{in}}$, e.g., from common laser timing, can be compressed by the chicane. Uncorrelated rf amplitude and phase fluctuations broaden the longitudinal phase space and are key parameters determining the beam timing jitter.

The electrical system that generates the cavity drive signal and the resulting rf fields is subject to electrical disturbances, which result in electrical noise. This electrical noise can often appear as spurs in the signal power spectral density and can be decomposed into phase and amplitude components [2]. Equations in this paper focus on phase noise; however, the same principles can be applied also to the amplitude component. There are three main sources of disturbances in the control system that operates the cavities: the detector (downconverter, DWC), the actuator (ACT), and the reference source (main oscillator, MO). The control system and its noise sources are analyzed within the formalism of a feedback loop, where the cavity is the plant [3,4].

Ideally, the control system ensures that the cavity field phase follows that of the reference, and consequently, the beam. To evaluate the control system's performance, the phase between the cavity field and the reference source,

*Contact author: frank.ludwig@desy.de

referred to as the residual phase, is introduced. This is important because in FELs, a single reference source is used to generate both the electron beam and the cavity field, which results in a common mode and residual rf field between them [5]. The cavity acts as a filter for rf signals, further mitigating the influence of the residual signal on beam jitter. The resulting rf field, referred to as the induced field, represents noise contributions induced onto the beam. The next Sec. I A aims to evaluate the impact of the three noise sources on the beam. Sections I B and I C introduce the different types of detectors, which primarily determine the performance of the control system and ultimately affect beam stability.

A. Noise contributions of rf control systems

When neglecting Lorentz force detuning and beam loading effects, the noise transfer functions of steady-state cavity regulation can be found by solving the system algebraically using small signal analysis in the Laplace domain. The result can be evaluated analytically or numerically for amplitude and phase noise [3]. As pointed out before, the major phase noise sources in the rf control system are the field detection $S_{\varphi,\mathrm{DWC}}$, actuator chain $S_{\varphi,\mathrm{ACT}}$, and the reference $S_{\varphi,\mathrm{MO}}$. As shown in [3], without taking latency into account, the power spectral density of the residual phase noise between the cavity field and reference for a proportional controller with gain $g_0 \gg 1$, $H_{\mathrm{DWC}}(s) \approx 1$, and offset frequency f results in

$$S_{\varphi,\mathrm{RES}}(f) = |\mathrm{HP}_{f'_{12}}(f)|^2\, S_{\varphi,\mathrm{MO}}(f) + |\mathrm{LP}_{f'_{12}}(f)|^2 \left[S_{\varphi,\mathrm{DWC}}(f) + \frac{1}{g_0^2} S_{\varphi,\mathrm{ACT}}(f) \right]. \tag{2}$$

Equation (2) shows that the residual phase noise between the cavity and the reference reflects the fact that the reference noise contribution $S_{\varphi,\mathrm{MO}}$ is filtered by a first-order high-pass $\mathrm{HP}_{f'_{12}}$ within the closed-loop bandwidth $f'_{12} = g_o f_{12}$, where f_{12} is the cavity half-bandwidth. The field detector $S_{\varphi,\mathrm{DWC}}$ and actuator noise $S_{\varphi,\mathrm{ACT}}$ are low-pass $\mathrm{LP}_{f'_{12}}$ filtered. Note that the requirements on the actuator chain are relaxed by $1/g_0^2$. Within the presented detection scheme in Sec. I C, Eq. (2) can also be used for the residual amplitude noise $S_{\alpha,\mathrm{RES}}(f)$ description.

The residual phase is defined by the phase difference between the cavity field and the reference source, but it does not fully capture the impact of the rf control system on the beam above the closed-loop bandwidth f'_{12}. The induced phase of the cavity field onto the beam is a more accurate metric, and it can be obtained by filtering the reference source by a low-pass characteristic $\mathrm{LP}_{f'_{12}}(f)$. This can be derived by using Eq. (7) from [3] with a proportional controller with $g_0 \gg 1$ and constant DWC transfer function. Combining both bandwidth regions, the overall jitter induced onto the beam from the rf control system results in

$$S_{\varphi,\mathrm{IND}}(f) = |\mathrm{HP}_{f'_{12}}(f)\mathrm{LP}_{f'_{12}}(f)|^2 S_{\varphi,\mathrm{MO}}(f) + |\mathrm{LP}_{f'_{12}}(f)|^2 \left[S_{\varphi,\mathrm{DWC}}(f) + \frac{1}{g_0^2} S_{\varphi,\mathrm{ACT}}(f) \right]. \tag{3}$$

The residual integrated timing jitter of the rf field $\sigma_t = \sigma_\varphi/(2\pi f_{\mathrm{rf}})$ and amplitude fluctuation σ_A/A within the bandwidth ΔB are given by

$$\sigma_\varphi = \sqrt{\int_{\Delta B} S_{\varphi,\mathrm{RES}}(f)\, df}, \qquad \frac{\sigma_A}{A} = \sqrt{\int_{\Delta B} S_{\alpha,\mathrm{RES}}(f)\, df}, \tag{4}$$

where f_{rf} is the cavity resonance frequency and A is the amplitude of the rf field. To achieve electron beam jitter below 100 as with a superconducting cavity at $f_{\mathrm{rf}} = 1.3$ GHz and half-bandwidth $f_{12} = 65$ Hz, the single-sideband (SSB) phase and amplitude noise floor must be below $-180\,\mathrm{dBc/Hz}$. With optimized controller gain, the high-power chain should be below $-140\,\mathrm{dBc/Hz}$ [6]. Thus, especially the field detection and the facility reference source are crucial.

B. Carrier-based rf control

Precision rf control systems providing sub-10 fs resolution are based on non-IQ sampling schemes for field detection by mixing the rf cavity signal to an intermediate frequency for digitization [6–8]. These heterodyne (HDR), carrier-based receivers provide many advantages—e.g., 360° detection, short-term stability, small PM to AM conversion, and phase noise varying between -150 and -160 dBc/Hz—and are implemented in various form factors. However, such systems suffer from 1/f noise, power limitations of front-end mixers, and relatively high ADC noise spectral densities [6]. rf control systems using carrier-based analog detection and processing can achieve better resolution, but, in general, suffer from the same limitations.

C. Carrier-suppressed-based rf control

To achieve attosecond resolution, receiver concepts have to be revised. Depending on the available signal power, interferometric methods demonstrate excellent short-term phase noise performance and achieve time resolutions in the 10 as range. Measurements have shown that all limitations of conventional receivers can be mitigated [9–12]. As shown in Fig. 1(a), a carrier suppression interferometer (CSI) uses destructive interference of the carrier signal before detecting the residual amplitude and phase noise of the device under test (DUT) by a conventional detection system.

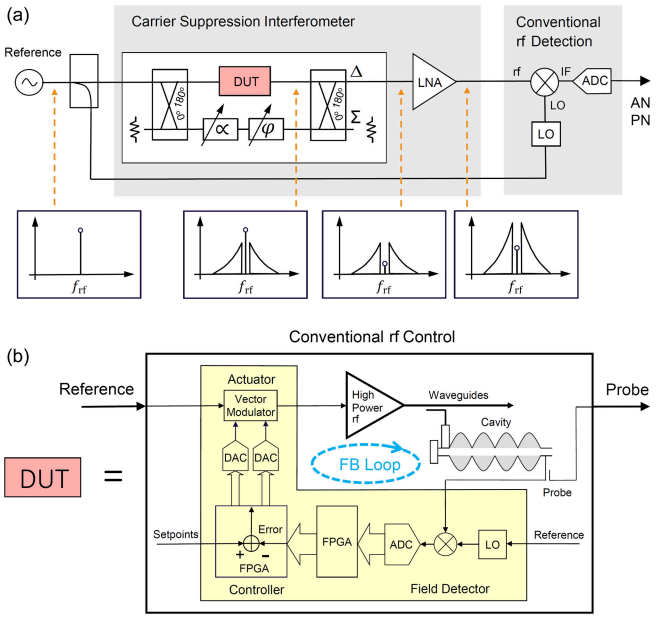

FIG. 1. (a) Simplified residual phase (PN) and amplitude noise (AN) measurement of a device under test (DUT) using a carrier suppression interferometer and (b) replacement of the DUT by a complete, carrier based, conventional rf control system.

The destructive interference is achieved by appropriate adjustment of attenuators and phase shifters, which reduce the carrier power, whereas the noise sidebands introduced by the DUT remain unchanged and can be amplified [10–12]. For sufficiently low carrier power, the 1/f noise added by the low-noise amplifier (LNA) [13] and the postdetection system can be neglected [9]. The phase noise contribution of the common reference source is subtracted and ideally vanishes. We demonstrate how to use this method in rf control for particle accelerator applications. As shown in Fig. 1(b), the DUT is replaced by a complete rf control system [14,15]. As in a residual measurement, the input of the DUT is the reference and its output is the cavity signal. The CSI detection, as an extended regulation branch, can control the cavity signal with much higher resolution. To continuously maintain destructive interference with the required suppression level, the method is better suited to accelerators with a continuous wave (cw) rather than a pulsed-rf mode of operation [16,17]. Due to the destructive interference, the phase of the carrier is not defined and the CSI detector has no carrier phase information. Because the information of the carrier's phase and amplitude is mandatory for rf feedback closed-loop operation, the rf field detection is a hybrid system comprised of a conventional and interferometric based receiver. This approach combines advantages of both receivers as pointed out in [6].

II. RF CONTROL SYSTEM AT CMTB

To demonstrate the applicability and performance of a CSI-based rf control system, tests were carried out at the

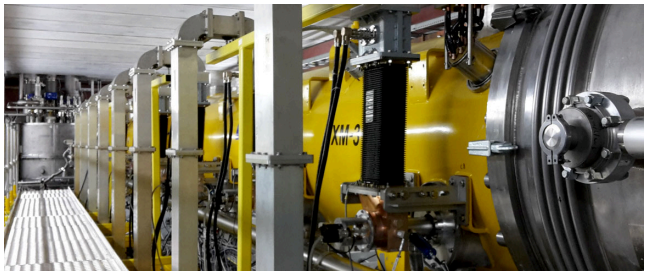

FIG. 2. Cryo Module Test Bench (CMTB) at DESY operating superconducting cavities with a half-bandwidth of 65 Hz.

Cryo Module Test Bench (CMTB) at DESY, shown in Fig. 2. We operated a single superconducting cavity with a half-bandwidth of 65 Hz, loaded quality factor $Q_L = 10^7$ at a gradient of 8 MV/m driven by an inductive output tube (IOT) in cw mode. Figure 3 depicts the structure of the rf controls used for the tests. The low-level rf (LLRF) system is a commercial MicroTCA.4 system [6,18], which houses conventional HDR detectors (CH1, CH2), digital processing, and an up-converter vector modulator (VM) to drive the cavity. The in-loop CSI signal uses a HDR detector (CH2) for postprocessing. The in-loop CSI detector measures the phase and amplitude difference between cavity probe and reference. The cavity probe signal with carrier is measured by a HDR detector (CH1). The out-of-loop CSI detector signal is converted to baseband and measures the rf regulation performance.

As a reference, an ultralow noise high-output power rf reference source or main oscillator (MO) developed by DESY, together with Warsaw University of Technology (WUT) was used. The rf reference source is meanwhile

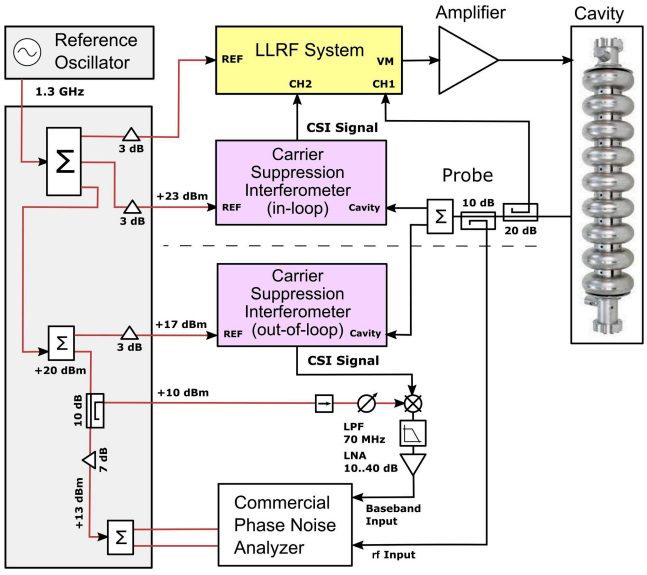

FIG. 3. rf controls structure extends a standard LLRF system with an in-loop CSI and out-of-loop CSI for performance verification.

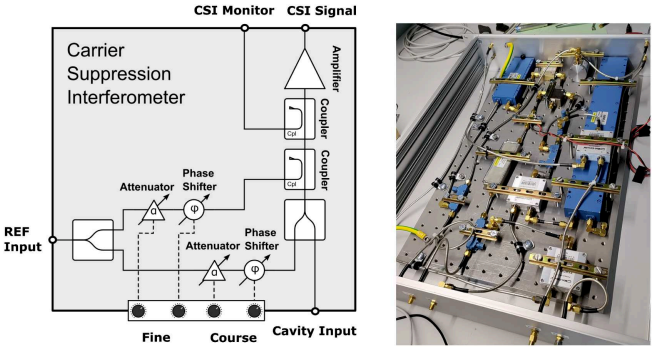

FIG. 4. Structure of the CSI module for rf controls. A coarse and fine adjustment branch provides the initial destructive interference.

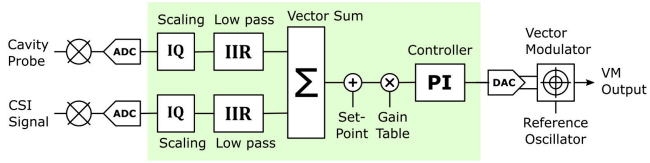

FIG. 5. LLRF firmware structure.

commercially available, see [19]. Figure 4 shows the structure of a CSI module packaged in a 19-inch unit providing the destructive interference and the phase and amplitude sidebands of interest. The CSI output signal is amplified by 40 dB with a low-noise amplifier (LNA) before being further processed in the LLRF detection system (CH2). Destructive interference is initially adjusted manually by a variable attenuator and a phase shifter (coarse and fine branch). Because the remainder of the carrier signal detected by the CSI is interpreted as an error, the feedback keeps the suppression automatically maximized. This is a great benefit of CSI applications in regulation systems. Both error signals from CH1 and CH2, using non-IQ sampling with digital downconversion, are combined in firmware, as shown in Fig. 5. The scaling factors are adjusted to maximize the influence of the CSI. The infinite impulse response (IIR) filters are used to reduce effects of the other passband modes of the cavity. The controller has a proportional and integral gain (PI). The realization of two independent controllers in combination with a frequency selective complementary digital filter might be an alternative approach.

III. PHASE NOISE CHARACTERIZATION

In this section, the most relevant noise sources of the LLRF system are identified and presented. To identify the limiting noise sources, the noise transfer function of each source contributing to the residual jitter of the rf control system is determined by numerical simulations.

A. Subsystems noise identification

Figure 6 shows absolute phase noise measurements of relevant rf control subsystems. These are the reference source (MO), in-loop field detector (CSI), actuator chain (ACT), cavity microphonics (MIC), and carrier-based field detector (HDR). For the phase noise of the HDR field detector, a parameterized data curve is used. The cavity microphonics is reconstructed by filtering the difference between the measured open-loop noise data and the reference. The phase noise of the reference oscillator (MO) is measured using a commercial phase noise analyzer [20]. Similarly, the actuator (ACT) was measured in open loop at the coupled IOT output port. The HDR detector was characterized in the laboratory [6], while the CSI detector was measured by feeding the reference into the REF input and cavity input port of the CSI (see Fig. 4).

The calibration was obtained by two methods such as rf power budget [9] and by determining the suppression factor [21]. The measured rf power at the DUT is equal to $+9.4$ dBm. Taking the 3.2 dB losses of the combiner into account, which provides the destructive interference, the estimated phase noise floor of the CSI has been determined to be -180.2 dBc/Hz, which is in good agreement with the measurement shown in Fig. 6. The integrated time resolution of the CSI detector is 112 as within a bandwidth of $[10\ \text{Hz}, 1\ \text{MHz}]$. Within the beam-relevant closed-loop bandwidth of 40 kHz, the CSI resolution is approximately 64 as. Under laboratory conditions, the HDR field detector has a resolution of less than 2 fs within the cavity closed-loop bandwidth of 40 kHz at -147 dBc/Hz. In this experiment its noise floor is slightly degraded, because of lower input rf power. All phase noise spectra have been measured with a commercial phase noise analyzer [20]

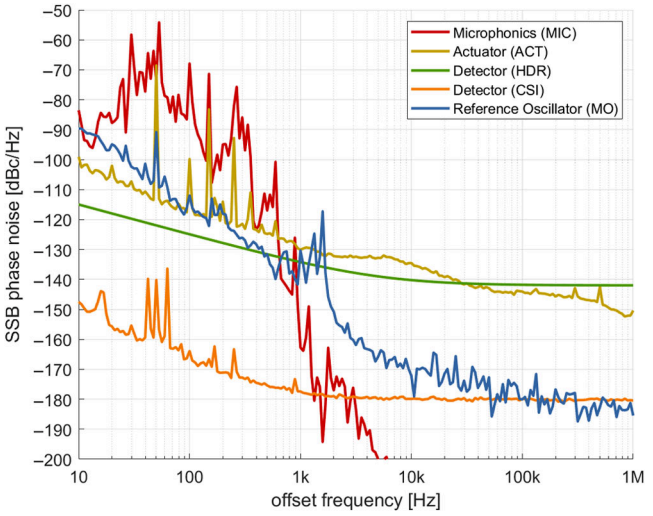

FIG. 6. Measured absolute phase noise of the relevant rf control subsystems. The measurement resolution of the CSI is 112 as within the bandwidth of $[10\ \text{Hz}, 1\ \text{MHz}]$ and 64 as within the closed-loop bandwidth of 40 kHz, respectively.

using cross correlation, which has a floor limitation of approximately −183 dBc/Hz and 1/f noise limitation of approximately −145 dBc/Hz at 100 Hz.

B. rf control noise simulations

The LLRF system was simulated with the MATLAB [22] control tool box. The block diagram of the simulation model is shown in Fig. 7. The system model consists of the main plant $H_{\mathrm{CAV}}(s)$ (superconducting cavity), the detector $H_{\mathrm{DWC}}(s)$ (field detector), $H_{\mathrm{ACT}}(s)$ (actuator), and the controller $G(s)$. Each subsystem is modeled by a first-order transfer function. Since the LLRF system is a digital control loop, the simulation uses discrete models in the z domain. For the simulation, the model parameters are defined in the s domain and then transferred into the z domain. The plant, in this case a nine-cell superconducting cavity, is modeled as a first-order system including latency. Other passband modes of such a cavity are not taken into account. Considering the modeling in the f domain, all subsystems' latency contributions can be summarized in one latency term that has been added to the cavity model. The controller is a standard PI controller of the form

$$G(s) = g_0 + \frac{2\pi f_i}{s}, \tag{5}$$

with a proportional gain g_0 and an integrator bandwidth f_i. The simulation result is a set of transfer functions shown in Fig. 8, namely, K_{MIC}, K_{ACT}, K_{HDR}, K_{CSI}, K_{MO}, which describe the contribution of each disturbance to the residual output $\varphi_{\mathrm{RES}}(s)$. Apart from the effects caused by the integrator of the controller and latency of the system, the transfer functions are in agreement with Eq. (2). According to [3], all individual phase noise contributions of each contributing subsystem can be determined by the individual noise spectral densities and transfer functions. Their sum yields the residual noise contribution $S_{\varphi,\mathrm{RES}}$. The induced phase noise $S_{\varphi,\mathrm{IND}}$ is defined by Eq. (3) and describes the impact onto the accelerated electron beam by the LLRF system.

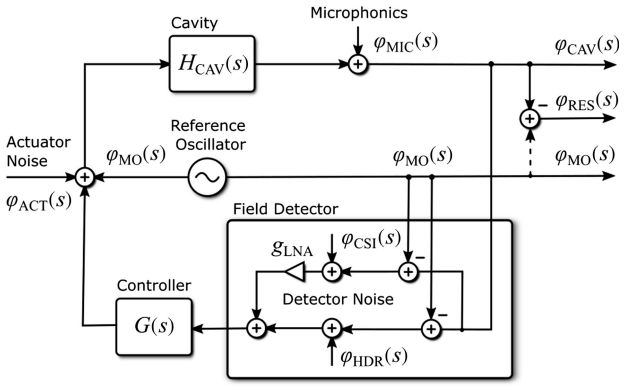

FIG. 7. Block diagram of the LLRF regulation system with all relevant noise sources. The field detector is a hybrid system based on a standard HDR and an interferometric CSI detector.

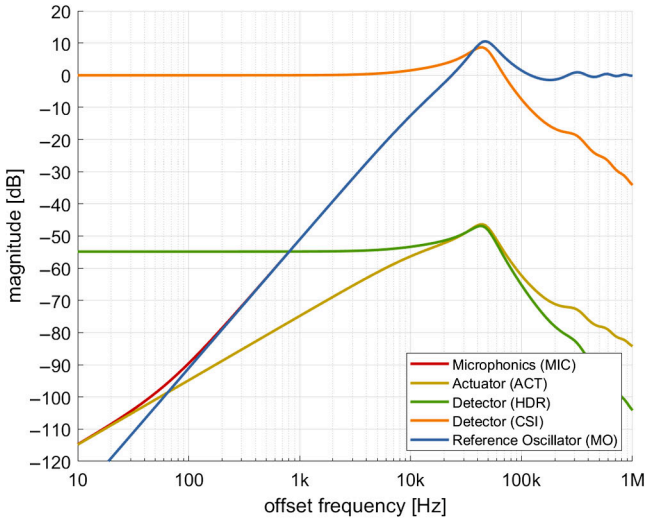

FIG. 8. Transfer functions of relevant noise sources contributing to the residual phase noise. Dominant contributors are the reference source (blue curve) and the CSI detector (orange curve). The cavity first-order cut-off frequency is $f_{12} = 65$ Hz, controller gain is $g_0 = 55$ dB with an integral bandwidth of $f_i = 10$ kHz, and the system latency time is $t_D = 3.5$ μs.

C. Residual noise contributions

Based on the numerically simulated noise transfer functions K_i with $i = \{\mathrm{MIC}, \mathrm{ACT}, \mathrm{HDR}, \mathrm{CSI}, \mathrm{MO}\}$ depicted in Fig. 7, the expected residual noise contributions are given by

$$S_{\varphi,\mathrm{RES},i}(f) = |K_i(f)|^2 S_{\varphi,i}(f), \tag{6}$$

where $S_{\varphi,i}(f)$ are the measured noise contributors presented in Fig. 6. The result is shown in Fig. 9. The total residual phase noise (gray curve)

$$S_{\varphi,\mathrm{RES}}(f) = \sum_i S_{\varphi,\mathrm{RES},i}(f) \tag{7}$$

is in good agreement with the measured residual phase noise (black curve). The actuator noise (yellow curve) and cavity microphonics (red curve) are well suppressed below the closed-loop bandwidth. In order to minimize the influence of the carrier-based HDR field detector (green curve), compared to the CSI detector (orange curve), a proper rf power adjustment is applied. Major contributions to the residual noise of the rf control (black curve) are caused by the reference source and the CSI detector around the closed-loop frequency f'_{12}. Above the closed-loop bandwidth, according to the low-pass filter of Eq. (2), the actuator and detector noise decrease with higher frequencies, whereas the residual noise follows the reference (blue curve). Considering the induced error on the beam in Eq. (3), the reference noise

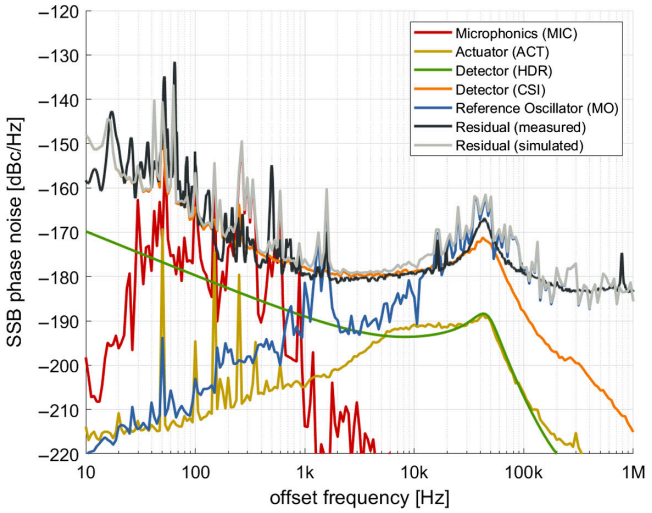

FIG. 9. Residual noise contributions of relevant noise sources. The reference source around the closed-loop frequency is identified as the crucial noise source. Controller parameters: proportional closed-loop gain 55 dB, integral bandwidth 10 kHz.

contribution rolls off due to the cavity filtering with the closed-loop bandwidth. The CSI detection floor can be further lowered by increasing the output power from the cavity. However, this power is constrained by the cavity design, as well as the power handling capabilities of the electronic components.

IV. CAVITY FIELD JITTER

In the previous section, various noise sources and their impact on the rf cavity field stability were discussed. To benchmark an rf control system using different in-loop detector types (HDR vs CSI), out-of-loop (OOL) measurements have been deployed. For OOL measurements a commercial phase noise analyzer (FSWP) [20] and an out-of-loop CSI detector were used in parallel. Phase noise spectra and integrated timing jitters are shown in Figs. 10(a) and 10(b). In open loop (blue curve), due to perturbations from the facility infrastructure, cavity microphonics dominate, and 0.6 ps time jitter is accumulated [10 Hz, 1 MHz] [23–25].

When the feedback is closed using the HDR detector (purple curve), the phase noise is dominated by the noise of the HDR detector. Even though laboratory measurements of the HDR detector show an integrated jitter of 2 fs (see Sec. III A), measurements at the facility show an integrated time jitter of more than 20 fs within the closed-loop bandwidth of 40 kHz. The main contributor is a low frequency distortion line at approximately 68 Hz, which is caused by the imperfect facility structure (vibration, grounding). At frequency 831 kHz, the $8\pi/9$ passband mode of the cavity is clearly visible and it can be further reduced by filtering.

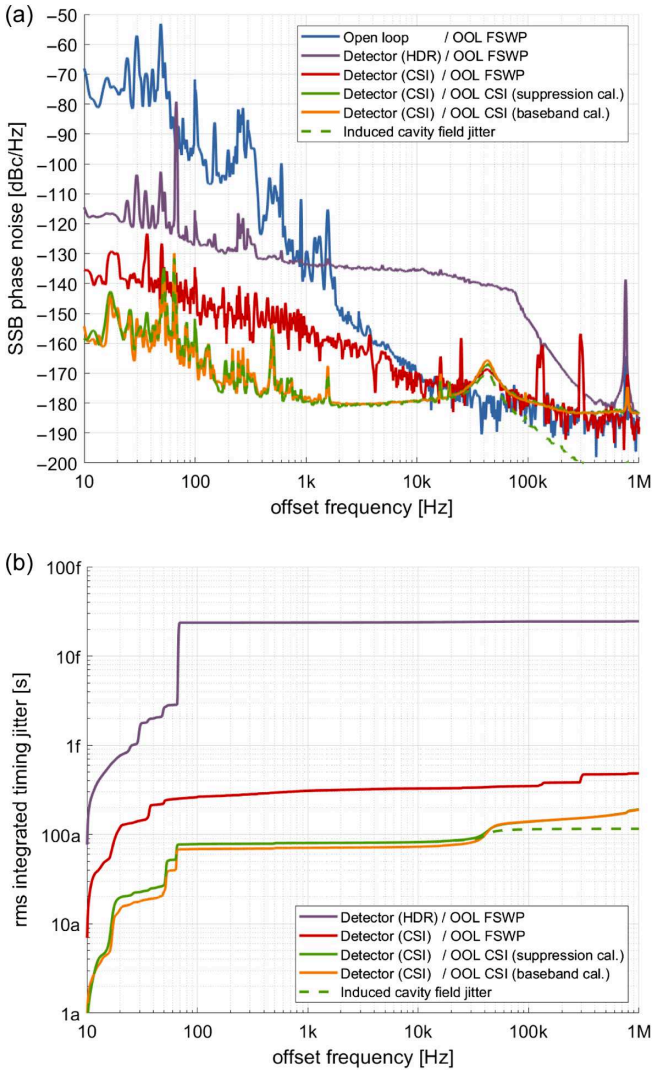

FIG. 10. (a) For the out-of-loop (OOL) measurements a commercial phase noise analyzer (FSWP) [20] or an OOL CSI is used and (b) integrated timing jitter performance of a hybrid rf control for different in-loop detectors. The integrated jitter of the cavity regulation within a bandwidth of [10 Hz, 1 MHz] is measured to be 189 as using a CSI detector. The dominant noise contribution is caused by the regulation's waterbed effect near maximum gain from the remaining reference noise. The induced cavity field jitter is expected to be about 116 as.

When using the CSI detector with less noise for the in-loop regulation, a higher suppression of the actuator noise and the cavity microphonics is achieved. Phase noise spectral densities (green and orange curves) around −160 dBc/Hz down to −180 dBc/Hz can be reached, resulting in ultralow noise timing jitter of the cavity. In Fig. 10(b), for low offset frequencies, the out-of-loop CSI detector (green and orange curve) shows an excellent integrated time jitter below 100 as. We used two independent measurements of the CSI out-of-loop detection. For the orange curve the baseband method (see Fig. 3) is applied, while for the green curve the method of

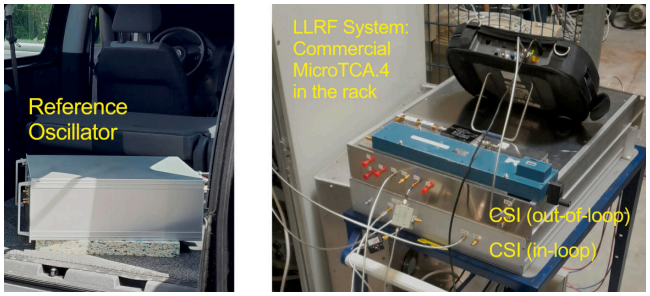

FIG. 11. Reference oscillator (left) was located outside the facility to reduce the influence of acoustic disturbances. The in-loop and out-of-loop CSI (right) are placed next to the rack, which houses the conventional LLRF system. On top of the modules, the baseband detection and a spectrum analyzer to track the quality of the carrier suppression are shown.

determining the suppression factor [21] is used. Even using cross-correlation techniques for out-of-loop measurements, a commercial phase noise analyzer (red curve) cannot resolve the performance of the CSI detector. For higher frequencies the waterbed peak near the maximum closed-loop frequency of about 40 kHz is a major contribution to the integrated jitter. The waterbed peak is caused by the latency t_D of the regulation system and occurs at the frequency $f_{12}\, g_{\max} = 1/4t_D$. The measured cavity regulation performance is 189 as over the full bandwidth of [10 Hz, 1 MHz]. These unprecedented results constitute a factor 10 improvement compared to state-of-the-art field detection in superconducting radio frequency (SRF) accelerator technology [26,27]. The experimental implementation of the setup is shown in Fig. 11.

The residual jitter is expected to be lower with smaller controller gains, when using better actuators and in the presence of less cavity microphonics. For frequencies above the closed-loop bandwidth, the cavity efficiently filters out noise of the reference and field detectors and this noise is not imprinted onto the beam. The green dashed line in Fig. 10(a) indicates the expected phase noise spectral density transferred to the beam, resulting in a total timing jitter of 116 as [see Fig. 10(b)]. Based on the analysis shown in Fig. 9, the phase noise of the reference source in the middle frequency range $[1\ \text{kHz}, 100\ \text{kHz}]$ was identified to be the most important contribution to the induced cavity time jitter. This imposes even tighter requirements for future oscillators with 1/f corners of about -180 dBc/ Hz below 1 kHz.

V. CONCLUSION

Hybrid rf control systems using carrier suppression detectors have the potential to control the cavity in accelerators with attosecond resolution. For an rf control system with a single superconducting cavity operating at 1.3 GHz in cw at CMTB, an integrated time jitter of 189 as within the frequency range $[10\ \text{Hz}, 1\ \text{MHz}]$ was demonstrated. This outperforms state-of-the-art short-term field stability of superconducting cavity rf fields by more than one order of magnitude. Noise contributions from the reference source are identified to be crucial on a floor of -180 dBc/Hz in the frequency range $[1\ \text{kHz}, 100\ \text{kHz}]$. The contribution was identified to originate from the regulation related waterbed effect. By filtering the noise through the cavity above the system's closed-loop bandwidth, the beam jitter is expected to be about 116 as. Demands for higher performance reference oscillators with reduced 1/f noise and improved high-power chains will grow. Further integration steps of the method into existing form factors are needed. The presented research combining conventional receiver techniques with carrier suppression detectors is well suited for cw operation and is an important milestone toward pump-probe experiments in the attosecond range.

ACKNOWLEDGMENTS

The research was financed by the Matter and Technology program, subtopic ARD-ST3, of the Helmholtz Association.

[1] H. Schlarb *et al.*, Next generation synchronization system for the VUV-FEL at DESY, in *Proceedings of the FEL'05* (JACoW, Geneva, Switzerland, 2005), MOPP036, pp. 118–121, https://jacow.org/f05/papers/MOPP036.pdf.

[2] E. Rubiola, *Phase Noise and Frequency Stability in Oscillators* (Cambridge University Press, Cambridge, England, 2009), 10.1017/CBO9780511812798.

[3] F. Ludwig *et al.*, Phase stability of the next generation RF field control for VUV- and x-ray free electron laser, in *Proceedings of the EPAC'06*, Series and Number European Particle Accelerator Conference No. 10 (JACoW, Geneva, Switzerland, 2006), pp. 1453–1455.

[4] S. Simrock and Z. Geng, *Low-Level Radio Frequency Systems* (Springer, New York, 2022), pp. 226–229.

[5] S. Simrock and Z. Geng, *Low-Level Radio Frequency Systems* (Springer, New York, 2022), pp. 240–242.

[6] F. Ludwig *et al.*, RF controls towards femtosecond and attosecond precision, in *Proceedings of the IPAC'19* (JACoW, Geneva, Switzerland, 2019), pp. 3414–3418.

[7] L. Doolittle *et al.*, Digital low-level rf control using non-IQ sampling, in *Proceedings of LINAC 2006, Knoxville, Tennessee* (JACoW Publishing, Geneva, Switzerland, 2006), pp. 568–570, https://jacow.org/l06/papers/THP004.pdf.

[8] O. Troeng and L. Doolittle, Low-latency digital downconversion for control applications, 10.48550/arXiv.2102.05906 (2021).

[9] L. Springer *et al.*, Phase noise measurements for L-band applications at attosecond resolution, IEEE Trans. Instrum. Meas. **71**, 1 (2022).

[10] E. Ivanov, M. Tobar, and R. Woode, Microwave interferometry: Application to precision measurements and noise reduction techniques, IEEE Trans. Ultrason. Ferroelectr. Freq. Control **45**, 1526 (1998).

[11] E. Rubiola and V. Giordano, A low-flicker scheme for the real-time measurement of phase noise, IEEE Trans. Ultrason. Ferroelectr. Freq. Control **49**, 501 (2002).
[12] E. Rubiola and V. Giordano, Advanced interferometric phase and amplitude noise measurements, Rev. Sci. Instrum. **73**, 2445 (2002).
[13] Narda—Miteq, LNA-40-01000200-07-10P, https://www.nardamiteq.com/docs/LNA-40-01000200-07-10P.PDF.
[14] H. Ma, M. Champion, M. Crofford, K.-U. Kasemir, M. Piller, L. Doolittle, and A. Ratti, Low-level rf control of spallation neutron source: System and characterization, Phys. Rev. ST Accel. Beams **9**, 032001 (2006).
[15] J. Branlard *et al.*, The European XFEL LLRF system, in *Proceedings of the IPAC'12* (JACoW, Geneva, Switzerland, 2012), pp. 55–57.
[16] A. Bellandi *et al.*, LLRF R&D towards cw operation of the European XFEL, in *Proceedings of the LINAC'18*, Series and Number Linear Accelerator Conference No. 29 (JACoW, Geneva, Switzerland, 2019), pp. 223–226.
[17] J. Branlard *et al.*, Status of cryomodule testing at CMTB for cw R&D, in *Proceedings of the SRF'19* (JACoW, Geneva, Switzerland, 2019), pp. 1129–1132.
[18] J. Branlard *et al.*, MTCA.4 LLRF system for the European XFEL, in *Proceedings of the 20th International Conference Mixed Design of Integrated Circuits and Systems—MIXDES 2013* (IEEE, New York, 2013), pp. 109–112, https://ieeexplore.ieee.org/document/6613323.
[19] KVG Quarz Crystal Technology GmbH, Main oscillator, https://kvg-gmbh.de/product/main-oscillator/ (2024).
[20] Rohde & Schwarz GmbH & Co.KG, FSWP, https://www.rohde-schwarz.com/de/produkte/messtechnik/phasenrauschmessplaetze/rs-fswp-phasenrausch-und-vco-messplatz_63493-120512.html.
[21] N. Shtin, S. Ojha, and A. Chenakin, Residual noise characterization using interferometric measurement technique, Anritsu Tech. Bull. **97**, 70 (2022), https://dl.cdn-anritsu.com/ja-jp/test-measurement/reffiles/About-Anritsu/R_D/Technical/97/97-10.pdf.
[22] MathWorks, Inc., MATLAB, https://www.mathworks.com/products/matlab.html.
[23] T. Powers *et al.*, Microphonics testing of LCLS II cryomodules AT JLAB, in *Proceedings of the SRF 2019* (JACoW, Geneva, Switzerland, 2019), pp. 493–497.
[24] A. Bellandi *et al.*, Narrow bandwidth active noise control for microphonics rejection in superconducting cavities at lLCLS-II, in *Proceedings of the 31st International Linear Accelerator Conference (LINAC'22)* (2022), pp. 785–788, 10.18429/JACoW-LINAC2022-THPOPA21.
[25] G. Davs *et al.*, Microphonics testing of the CEBAF upgrade 7-cell cavity, in *Proceedings of the PAC-2001* (IEEE, New York, 2001).
[26] C. Serrano *et al.*, RF controls for high-QL cavities for the LCLS-II, in *Proceedings of the IPAC'18* (JACoW, Geneva, Switzerland, 2018), pp. 2929–2933.
[27] K. Zenker *et al.*, MicroTCA.4-based low-level rf for continuous wave mode operation at the ELEB accelerator, IEEE Trans. Nucl. Sci. **68**, 2326 (2021).